

# Fast and Slow Blowup in the $S^2$ Sigma Model and (4+1)-Dimensional Yang-Mills Model\*

Jean Marie Linhart<sup>†</sup>      Lorenzo A. Sadun<sup>‡</sup>

November 21, 2018

## Abstract

We study singularity formation in spherically symmetric solutions of the charge-one and charge-two sector of the (2+1)-dimensional  $S^2$   $\sigma$ -model and the (4+1)-dimensional Yang-Mills model, near the adiabatic limit. These equations are non-integrable, and so studies are performed numerically on rotationally symmetric solutions using an iterative finite differencing scheme that is numerically stable. We evaluate the accuracy of predictions made with the geodesic approximation. We find that the geodesic approximation is extremely accurate for the charge-two  $\sigma$ -model and the Yang-Mills model, both of which exhibit fast blowup. The charge-one  $\sigma$ -model exhibits slow blowup. There the geodesic approximation must be modified by applying an infrared cutoff that depends on initial conditions.

Mathematics Subject Classification: 35-04, 35L15, 35L70, 35Q51, 35Q60  
Physics and Astronomy Classification: 02.30.Jr, 02.60.Cb

---

\*This work was partially supported by the Texas Advanced Research Program, and carried out at the University of Texas.

<sup>†</sup>Applied Science Fiction; 8920 Business Park Drive; Austin, TX 78759;  
jlinhart@asf.com.

<sup>‡</sup>Department of Mathematics; University of Texas at Austin; Austin, TX 78712;  
sadun@math.utexas.edu

# 1 Introduction, Background and Results

The geodesic approximation [7] is a popular tool for theorizing on the dynamics of systems with known spaces of stationary solutions. As the velocity tends toward zero, evolution should occur close to geodesics on the space of the stationary solutions.

But do equations in fact evolve as the geodesic approximation predicts?

We study three systems to which the geodesic approximation has been applied. We study the charge-one sector of the (2+1)-dimensional  $S^2$   $\sigma$ -model (hereafter referred to as the “charge-one  $\sigma$ -model”), the charge-two sector of the (2+1)-dimensional  $S^2$   $\sigma$ -model (the “charge-two  $\sigma$ -model”), and the (4+1)-dimensional Yang-Mills model. The  $S^2$   $\sigma$ -model is sometimes called the  $O(3)$   $\sigma$ -model or the  $\mathbb{CP}^1$  model, and the localized solutions are called “lumps”. In all cases the geodesic approximation suggests that localized solutions should shrink to zero size (“blow up”) in finite time.

Blowup phenomena can be categorized as “fast” or “slow”. In slow blowup, all relevant speeds go to zero as the singularity is approached. In fast blowup the relevant speeds do not go to zero. Shatah and Struwe [10] proved that there cannot be spherically symmetric fast blowup in the charge one  $\sigma$ -model. In particular, the approach to blowup cannot be asymptotically self-similar, as suggested by the geodesic approximation. This theorem does not apply to the charge-two  $\sigma$ -model, or to the (4+1)-dimensional Yang-Mills system.

In each case, we model the equations in a simple and robust numerical scheme for which the stability can be verified. Then we know the numerical scheme does not add features to the evolution of the differential equation. Consequently, we can make meaningful comparisons of the predictions of the geodesic approximation with the actual evolution of these equations. We observe slow blowup in the charge one  $\sigma$ -model, and fast blowup in the charge-two  $\sigma$ -model and the Yang-Mills model, in accordance with the Shatah-Struwe theorem.

This is not the first paper to numerically observe blowup in these models. However, our intent is not merely to confirm blowup. We quantify the deviations of the true trajectories from the geodesic approximation, in particular for the charge-one  $\sigma$ -model, where these deviations are substantial. We also suggest a modification of the geodesic approximation for the charge-one  $\sigma$ -model, applying a dynamically generated cutoff to certain integrals to obtain dramatically improved accuracy. In the charge-two  $\sigma$ -model and the Yang-

Mills model, we find that the geodesic approximation is extremely accurate, and no such modification is needed.

The literature on  $\mathbb{C}\mathbb{P}^1$  lump dynamics is extensive, especially in the charge-one sector, and begins with Ward's suggestion [14] of applying Monton's geodesic approximation [7] to this problem. The dynamics of lump scattering, in this approximation, were studied in depth by Leese [4] and Zakrzewski [15] on  $\mathbb{R}^2$ , and by Speight on  $S^2$  [11] and on other Riemann surfaces [12].

In 1990, Leese, Peyrard and Zakrzewski [5] studied the stability of numeric solitons, using a square grid and the traditional Runge-Kutta numerical approach, and found that lumps on a discretized system are inherently subject to shrinkage. This is of direct physical interest, since many physical systems (e.g., an array of Heisenberg ferromagnets) are naturally discretized. However, it raises the questions of whether a different discretization might avoid introducing spontaneous shrinking. In this paper we exhibit one that does.

The results of [5] also demonstrate the importance of doing a careful stability analysis of whatever numerical scheme one applies, to separate properties of the underlying differential equations from phenomena introduced by the discretization. The numerical methods of this paper were chosen to make such analysis possible [6].

The most important numerical test of the geodesic approximation of blowup, for the rotationally symmetric charge-one  $\sigma$ -model, was done by Piette and Zakrzewski [8]. In the charge-one sector, the Lagrangian for lump dynamics in the geodesic approximation has an infrared log divergence. To remedy this, Piette and Zakrzewski cut off their integrals at a large distance  $R$ , computed trajectories, and then took the  $R \rightarrow \infty$  limit. This procedure predicts fast blowup ( $a(t) \sim t_0 - t$ , where  $a(t)$  is the size of the lump at time  $t$ ), contradicting the Shatah-Struwe theorem. This prediction is also in mild contradiction of Piette and Zakrzewski's numerical results. They found that  $a(t)$  shrank slightly slower than linear, which they modeled as a power law with exponent slightly greater than one.

More recently, Bizoń, Chmaj and Tabor studied the universality of blowup in the charge-one  $\sigma$ -model [2]. They provide numerical evidence that the existence of blowup does not depend on the initial conditions (as long as there is enough energy), that the shape of the lump prior to blowup is universal, that the rate of blowup is slow ( $da/dt \rightarrow 0$  as  $t \rightarrow t_0$ ) but that the rate is dependent on initial conditions.

In this paper, we extend the results of [8] in several ways. First, we obtain

more accurate numerical data on the rate of blowup. We see that blowup in the rotationally symmetric charge-one  $\sigma$ -model deviates from linear by a log correction, not a power law. Second, we show that this can be understood within the framework of the geodesic approximation. The cutoff Lagrangian of [8] gives the correct dynamics if we do *not* take the  $R \rightarrow \infty$  limit. Rather,  $R$  should be understood as a dynamically generated cutoff that depends on the initial conditions. ( $R$  is of order  $|a(0)/a'(0)|$ ). The resulting trajectories are qualitatively similar to those found by Speight for lump dynamics on a sphere [11]. The difference is that Speight's cutoff (the radius of the sphere) is independent of initial conditions, while ours is fundamentally dynamic.

Third, we show how the shape of the lump depends on the speed of its shrinkage. In the geodesic approximation, the lump at all times looks like a static solution to the equations. We show that this is only approximately correct, and we quantify the deviations. In particular, we see that, shortly before blowup, lumps have the property that a small disk around the origin maps onto all of the target  $S^2$ .

Finally, we model the charge-two  $\sigma$ -model and the Yang-Mills model as a comparison to the charge-one  $\sigma$ -model. The form of the equations, the method of discretization, and the numerical stability analysis are similar for all three models. The conventional wisdom is that the Yang-Mills model should behave much like the charge-two  $\sigma$ -model, and this is borne out by our numerics. Moreover, in both these cases the rate of blowup is extremely close to that predicted by the geodesic approximation. This gives a standard of accuracy by which to judge the charge-one  $\sigma$ -model. To wit, the deviations from prediction on the charge-one  $\sigma$ -model are much, much larger and are not due to numerical error.

This paper is organized as follows. The  $S^2$   $\sigma$ -model and the Yang-Mills model are reviewed in Section 2. In Section 3 we present our method for numerically integrating the PDEs, and discuss the stability and accuracy of this method. Our results appear in Section 4, first for the charge-one  $\sigma$ -model, then for the charge-two  $\sigma$ -model, and finally for the Yang-Mills model.

## 2 Equations being modeled

### 2.1 The 2-dimensional $S^2$ $\sigma$ -Model

The two-dimensional  $S^2$   $\sigma$ -model has been studied extensively over the past few years in [4], [8], [5],[11], [12], [14], [15] and [3].

It is a good toy model for studying two-dimensional analogues of elementary particles in the framework of classical field theory. Elementary particles are described by classical extended solutions of this model, called lumps. Such lumps can be written down explicitly in terms of rational functions. This model is extended to (2+1) dimensions. The previous lumps are static or time-independent solutions, and, with the added dimension, the dynamics of these lumps are studied. The time dependent solutions cannot be constructed explicitly, so in (2+1)-dimensions studies are performed numerically, and analytic estimates are made by cutting off the model outside a radius  $R$ .

We will see that the  $S^2$   $\sigma$ -model displays both slow blowup and fast blowup. The charge-one  $\sigma$ -model exhibits logarithmic slow blowup, whereas the charge-two  $\sigma$ -model and the similar Yang-Mills (4+1)-dimensional model exhibit fast blowup.

Identifying  $S^2 = \mathbb{CP}^1 = \mathbb{C} \cup \{\infty\}$  we can write the Lagrangian density in terms of a complex scalar field  $u$ :

$$L = \int_{\mathbb{R}^2} \frac{|\partial_t u|^2}{(1 + |u|^2)^2} - \frac{|\nabla u|^2}{(1 + |u|^2)^2}. \quad (1)$$

The calculus of variations on this Lagrangian in conjunction with integration by parts yields the following equation of motion for the  $\mathbb{CP}^1$  model:

$$(1 + |u|^2)(\partial_t^2 u - \partial_x^2 u - \partial_y^2 u) = 2\bar{u}((\partial_t u)^2 - (\partial_x u)^2 - (\partial_y u)^2) \quad (2)$$

Here  $\bar{u}$  represents the complex conjugate of  $u$ .

We will look at the evolution of these equations near the space of static solutions. The static solutions are outlined in [14] among others. The entire space of static solutions can be broken into finite dimensional manifolds  $\mathcal{M}_n$  consisting of the harmonic maps of degree  $n$ . If  $n$  is a positive integer, then  $\mathcal{M}_n$  consists of the set of all rational functions of  $z = x + iy$  of degree  $n$ . We restrict our attention to  $\mathcal{M}_1$  and  $\mathcal{M}_2$ , the charge-one sector and the charge-two sector. On these two sectors the static solutions (with  $u(\infty)$  finite) all

have the form

$$u = \alpha + \frac{\beta}{z + \gamma} \quad (3)$$

and

$$u = \alpha + \frac{\beta z + \gamma}{z^2 + \delta z + \epsilon}, \quad (4)$$

respectively, depending on up to five complex parameters  $\alpha, \beta, \gamma, \delta, \epsilon$ . To simplify further, we impose rotational symmetry on the solution, which is respected by (2). For this regime the (2+1)-dimensional model reduces to a (1+1) dimensional model. These solutions become

$$\frac{\beta}{z} \text{ (on } \mathcal{M}_1) \text{ and } \frac{\gamma}{z^2} \text{ (on } \mathcal{M}_2), \quad (5)$$

with  $\beta$  and  $\gamma$  real. Note that by applying rotational symmetry we have also forced  $u(\infty)$  to be zero.<sup>1</sup> The geodesic approximation predicts that solutions evolve close to

$$\frac{\beta(t)}{z} \text{ or } \frac{\gamma(t)}{z^2}. \quad (6)$$

This paper is about the actual evolution of these equations. Instead of looking at  $\beta(t)$  or  $\gamma(t)$ , we look for the most general rotationally symmetric solution to (2). We find the evolution of:

$$\frac{f(r, t)}{z} \text{ or } \frac{f(r, t)}{z^2}. \quad (7)$$

The difference between the actual evolution of  $f(0, t)$  and that predicted in the geodesic approximation, and the difference between the profile  $f(r, t)$  (with  $t$  fixed) from  $\beta(t)$  (which is constant with respect to  $r$ ) gives us a means to gauge how accurately the evolution of this equation can be modeled by the geodesic approximation.

It is straightforward to calculate the evolution equation for  $f(r, t)$ . For  $u = \frac{f(r, t)}{z}$  it is:

$$\partial_t^2 f = \partial_r^2 f + \frac{3\partial_r f}{r} - \frac{4r\partial_r f}{f^2 + r^2} + \frac{2f}{f^2 + r^2} ((\partial_t f)^2 - (\partial_r f)^2). \quad (8)$$

---

<sup>1</sup>There are also rotationally symmetric static solutions with  $u(\infty) = \infty$ . Since the equations of motion are invariant under the transformation  $u \rightarrow 1/u$ , these behave identically to the solutions discussed here, and do not have to be considered separately.

For  $u = \frac{f(r, t)}{z^2}$  it is:

$$\partial_t^2 f = \partial_r^2 f + \frac{5\partial_r f}{r} - \frac{8r^3 \partial_r f}{f^2 + r^4} + \frac{2f}{f^2 + r^4} ((\partial_t f)^2 - (\partial_r f)^2). \quad (9)$$

In both cases the static solutions are  $f(r, t) = \text{constant}$ . In the charge-one sector this constant is the length scale, while in the charge-two sector it is the square of the length scale. In the geodesic approximation,  $f(r, t)$  depends on  $t$  but not on  $r$ . Blowup occurs when the length scale becomes zero, that is  $f(0, t) = 0$ . Even apart from the geodesic approximation, a singularity appears when  $f(0, t) = 0$ . This is what we call the instant of blowup.

Note that there is nothing singular about  $f(r, t)$  equaling zero when  $r \neq 0$ . That merely indicates that  $u$  maps the entire circle  $z = re^{i\theta}$  to the south pole of  $S^2$ . We shall see that this always happens, for smaller and smaller values of  $r$ , shortly before blowup.

## 2.2 The Yang-Mills Model

The Yang-Mills Lagrangian in 4 dimensions is a generalization of Maxwell's equations in a vacuum, and is discussed at length in [1]. We can regard this problem as being that of a motion of a particle, where we wish our particles to have certain internal and external symmetries, which give rise to the various geometrical objects in the problem. The states of our particles are given by gauge potentials or connections, denoted  $A$ , on  $\mathbb{R}^4$ , and we identify  $\mathbb{R}^4$  with the quaternions  $\mathbb{H}$ :  $\vec{x} = x_1 + x_2i + x_3j + x_4k$ . The gauge potentials have values in the Lie algebra of  $SU(2)$  which can be viewed as purely imaginary quaternions. The curvature  $F_{ij} = \partial_i A_j - \partial_j A_i + [A_i, A_j]$ , where  $[A_i, A_j] = A_i A_j - A_j A_i$  is the bracket in the Lie Algebra, gives rise to the potential  $V(A) = |F_{ij}|^2$  which is a nonlinear function of  $A$ . The static action is:

$$S = \frac{1}{2} \int |F_{ij}|^2 d^4 \vec{x}. \quad (10)$$

The space of finite-action configurations breaks up into topological sectors, indexed by the instanton number. We are interested in the sector with instanton number one. The local minima of (10) are the instantons on 4 dimensional space.

We now introduce a time variable  $t$  and consider the wave equation generated by this potential with Lagrangian:

$$L = \frac{1}{2} \int |\partial_t A_i|^2 - \frac{1}{2} |F_{ij}|^2 d^4 \vec{x}. \quad (11)$$

Via the calculus of variations, the evolution equation for this dynamical model is<sup>2</sup>

$$\partial_t^2 A_i = -\nabla_j F_{ij}. \quad (12)$$

Theoretical work on the validity of the geodesic approximation for an analogous problem, the monopole solutions to the Yang-Mills-Higgs theory on  $(3+1)$ -dimensional Minkowski space, is presented in [13].

The static solutions to equation (12) are simply the 4 dimensional instantons investigated in [1]. All degree one instantons take the form:

$$A(x) = \frac{1}{2} \left\{ \frac{(\bar{x} - \bar{a})dx - d\bar{x}(x - a)}{\lambda^2 + |x - a|^2} \right\} \quad x = x_1 + x_2 i + x_3 j + x_4 k \in \mathbb{H}. \quad (13)$$

We will consider connections the form

$$A(r, t) = \frac{1}{2} \left\{ \frac{\bar{x}dx - d\bar{x}x}{f(r, t) + r^2} \right\} \quad r = \sqrt{x_1^2 + x_2^2 + x_3^2 + x_4^2}. \quad (14)$$

This is the most general form of a rotationally symmetric connection. We will derive an equation of motion for  $f(r, t)$  from (12).

To get at this, start with connections of the form

$$A(r, t) = \frac{1}{2} g(r, t) \{ \bar{x}dx - d\bar{x}x \}. \quad (15)$$

One can then use (12) to calculate the differential equation for  $g$ :

$$\partial_t^2 g = 12g^2 + \frac{5\partial_r g}{r} + \partial_r^2 g - 8g^3 r^2. \quad (16)$$

---

<sup>2</sup>Note that we have defined  $A = (A_1, A_2, A_3, A_4)$  to be a time-dependent connection on  $\mathbb{R}^4$ , not a connection on  $\mathbb{R}^{4+1}$ . However, the dynamics of Yang-Mills connections on  $\mathbb{R}^{4+1}$  is almost identical. In that model,  $A = (A_0, A_i)$  and the  $|\partial_t A_i|^2$  term in the Lagrangian (11) is replaced by  $|F_{0i}|^2$ . After obtaining the equations of motion we apply the gauge choice  $A_0 = 0$ . The equations of motion then reduce to (12), plus a Gauss' Law constraint  $\partial_t(\partial_i A_i) = 0$  that comes from varying the Lagrangian with respect to  $A_0$ . This constraint is identically satisfied by the ansatz (14). Our results therefore apply to this model as well as to time-dependent connections on  $\mathbb{R}^4$ .



Substituting  $g(r, t) = (f(r, t) + r^2)^{-1}$ , we obtain a differential equation for  $f(r, t)$ :

$$\partial_t^2 f = \partial_r^2 f + \frac{5\partial_r f}{r} - \frac{8\partial_r f r}{f + r^2} + \frac{2}{f + r^2} ((\partial_t f)^2 - (\partial_r f)^2). \quad (17)$$

As with the charge-two sigma model, the static solutions are  $f(r, t) = \text{constant}$ , where the constant is the square of the length scale, and the geodesic approximation states that solutions should progress as  $f(r, t) = \alpha(t)$ . As before, blowup means  $f(0, t) = 0$ .

### 3 Numerical Method

A finite difference method is used to compute the evolution of these partial differential equations (8, 9, 17) numerically. Centered differences are used consistently except for

$$\partial_r^2 f + \frac{3\partial_r f}{r} \quad \text{and} \quad \partial_r^2 f + \frac{5\partial_r f}{r}. \quad (18)$$

In order to avoid serious instabilities in (8, 9, 17) these are modeled in a special way. Let

$$\mathcal{L}_1 f = r^{-3}(\partial_r)r^3(\partial_r)f = \partial_r^2 f + \frac{3\partial_r f}{r} \quad (19)$$

and

$$\mathcal{L}_2 f = r^{-5}(\partial_r)r^5(\partial_r)f = \partial_r^2 f + \frac{5\partial_r f}{r}. \quad (20)$$

These operators have negative real spectrum, hence they are stable. The naïve central differencing scheme on (18) results in unbounded growth at the origin, but the natural differencing scheme for this operator does not. For the first it is

$$\mathcal{L}_1 f \approx r^{-3} \left[ \frac{\left(r + \frac{\delta}{2}\right)^3 \left(\frac{f(r+\delta) - f(r)}{\delta}\right) - \left(r - \frac{\delta}{2}\right)^3 \left(\frac{f(r) - f(r-\delta)}{\delta}\right)}{\delta} \right]. \quad (21)$$

The second is done analogously.

With the differencing explained, we want to derive  $f(r, t + \Delta t)$ . We always have an initial guess at  $f(r, t + \Delta t)$ . In the first time step it is  $f(r, t + \Delta t) = f(r, t) + v_0 \Delta t$  with  $v_0$  the initial velocity given in the problem. On subsequent time steps the initial guess is  $f(r, t + \Delta t) = 2f(r, t) - f(r, t - \Delta t)$ . The appropriate forward time step can be used to compute  $\partial_t f(r, t)$  on the right hand side of (8, 9, 17). Then this allows us to solve for a new  $f(r, t + \Delta t)$  in the differencing for the second derivative  $\partial_t^2 f(r, t)$ . This procedure can be iterated several times to get increasingly accurate values of  $f(r, t + \Delta t)$ . In (17), for example, we iterate the equation:

$$f(r, t + \Delta t) = 2f(r, t) - f(r, t - \Delta t) + (\Delta t)^2 \left[ \partial_r^2 f(r, t) - \frac{5\partial_r f(r, t)}{r} - \frac{2(\partial_t f(r, t))^2}{f(r, t) + r^2} - \frac{2(\partial_r f(r, t))^2}{f(r, t) + r^2} - \frac{8\partial_r f(r, t)r}{f(r, t) + r^2} \right], \quad (22)$$

where all derivatives on the right hand side are represented by the appropriate differences.

There remains the question of boundary conditions. At the origin, in all models,  $f(r, t)$  is presumed to be a quadratic function, and this gives

$$f(0, t) = \frac{4}{3}f(\Delta r, t) - \frac{1}{3}f(2\Delta r, t). \quad (23)$$

At the  $r = R_{max}$  boundary we use Neumann boundary conditions  $\partial_r f(R_{max}, t) = 0$ . We essentially have a free wave equation outside of this boundary in all of the equations. This boundary condition allows information that has propagated out to it to bounce back toward the origin, but it does not permit information to come in through the boundary from infinity.

In the models generated from (9, 17), results indicate that the appropriate form for  $f(r, t)$  at any given time  $t$ , is a parabola in  $r$ , rather than a straight line. When looking at this aspect of the model, the  $f(R_{max}, t)$  boundary condition was changed to respect the parabola:

$$\partial_r f(R_{max}, t) = \partial_r f(R_{max} - \Delta r, t) \frac{R_{max}}{R_{max} - \Delta r}. \quad (24)$$

### 3.1 Stability and Accuracy

A lengthy analysis of the stability of the numerical schemes for (8, 17) is performed in [6]. That for (9) should be directly analogous to that for (17).

We do not wish to go into the full details of the analysis for the stability or convergence in this paper, as they are tedious.

However, we do emphasize the importance of such an analysis.

Discrete numerical models, such as these, are usually approximations to a desired continuum model. Usually the true continuum solution is only obtained as some parameter goes to zero or to infinity. In evaluating a model numerically, we introduce error. We have the unavoidable round off error that comes with every computer model, and also a truncation error that occurs from only taking finitely many terms.

Sometimes a method that seems otherwise favorable has undesired behavior that is caused by the discretization used in the problem.

For example, questions arise from [5] about the stability of the lumps for (8). They found that a soliton would shrink without perturbation from what should be the resting state. This seems to be a function of the numerical scheme used for those experiments. The numerical scheme used here for equations (8, 9, 17) has no such stability problems. Experiments show that a stationary solution is indeed stationary unless perturbed by the addition of an initial velocity.

In unstable numerical schemes, the roundoff error can come to be commingled with the calculation at an early stage and can then be magnified until it overcomes the true answer. A good, basic discussion of stability and numerical schemes can be found in [9].

Apart from the stability analysis, one can measure the effect of the spatial discretization by tracking different trajectories with identical initial conditions, a small fixed  $\Delta t$ , and a varying  $\Delta r$ . Any scheme will break down when the system develops important features that are too small compared to  $\Delta r$ . When two trajectories start to differ, that implies that the computation with the larger value of  $\Delta r$  has started to break down.

We see this in Figure 1, where we track  $f(0, t)$  for the charge-one  $S^2$   $\sigma$ -model. We pick input parameters of  $f(r, 0) = f_0 = 1.0$ ,  $\partial_t f(r, 0) = v_0 = -0.01$ , and  $\Delta t = 0.001$ . We track evolution with  $\Delta r = 0.1$ ,  $\Delta r = 0.05$  and  $\Delta r = 0.01$ . The difference between  $f(0, t)_{\Delta r=0.1}$  and  $f(0, t)_{\Delta r=0.01}$  at the point of blowup (specifically, when  $f(0, t)_{\Delta r=0.01}$  hits zero) is less than 0.01. This is considerably less than the grid size difference of 0.09. Furthermore, the difference when  $f(0, t)_{\Delta r=0.1} = 0.1$  is smaller still, with  $|f(0, t)_{\Delta r=0.1} - f(0, t)_{\Delta r=0.01}| \approx 0.002$ . This correspondence in the three trajectories indicates that the influence of the grid size on the features of the model can be ignored until  $f(0, t)$  has shrunk roughly to size  $\Delta r$ .

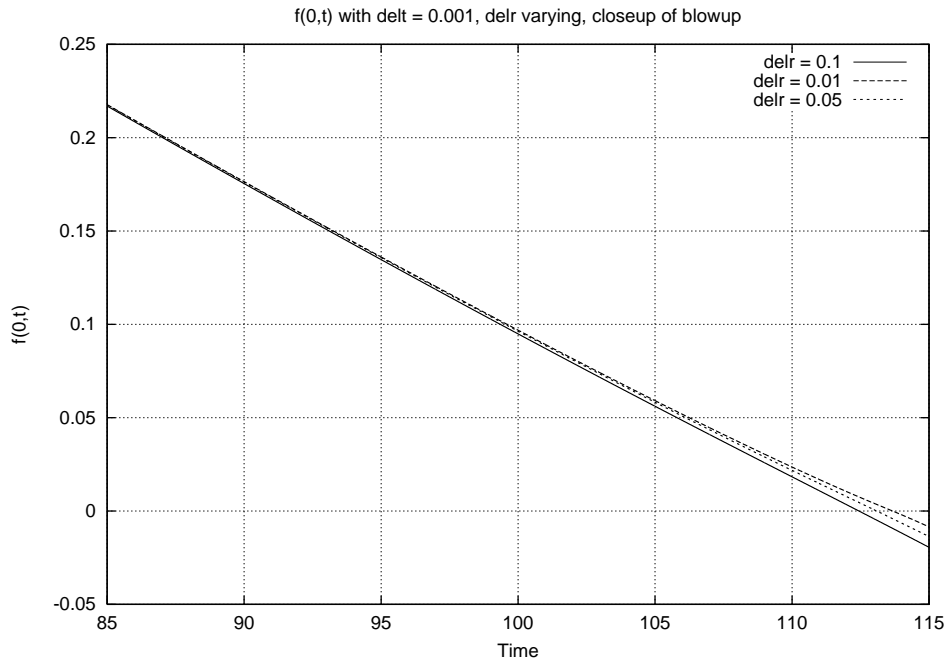


Figure 1: Different trajectories for different  $\Delta r$  values in the charge-one  $\sigma$ -model. We have zoomed in on a neighborhood of the blowup time in order to be able to see where these trajectories begin to deviate from one another.

## 4 Comparison to the Geodesic Approximation

We wish to compare the actual evolution of the blowup of the charge-one and charge-two  $S^2$   $\sigma$ -models and the Yang-Mills model with that predicted by the geodesic approximation.

In our ansatz for all three models, we model the evolution of  $f(r, t)$ , and in all cases the geodesics on the moduli space of stationary solutions are  $f(r, t) = \alpha(t)$ . When we calculate deviations from the geodesic approximation of this profile, we calculate deviations between the actual shape  $f(r, T)$ , with  $T$  fixed, and  $f(r, T) = \alpha$ . Note also that outside of a sufficiently large ball about the origin, all three equations are well approximated by the linear wave equation  $\partial_t^2 f = \partial_r^2 f$ . The interesting behavior should occur near the origin, and so evolution toward blowup is tracked as the evolution of  $f(0, t)$ .

## 4.1 Charge-One $S^2$ $\sigma$ -Model

For the charge-one  $S^2$   $\sigma$ -model, our calculations follow those done in [8] and [11].

In [8] the time evolution of blowup via the shrinking of lumps was studied. The Lagrangian was cut off outside of a ball of radius  $R$ , to prevent logarithmic divergence of the integral for the kinetic energy, and then an analysis of what happens in the  $R \rightarrow \infty$  limit was performed. In [11] the problem of the logarithmic divergence in the kinetic energy integral is solved by investigating the model on the sphere  $S^2$ . The radius of the sphere determines a parameter for the size analogous to the parameter  $R$  for the size of the ball the Lagrangian is evaluated on in [8].

Equation (1) gives us the Lagrangian for the general version of this problem. In the spherically symmetric geodesic approximation for the charge-one sector, we consider functions of the form

$$u = \frac{\beta}{z}. \quad (25)$$

If we restrict the Lagrangian to this space we get an effective Lagrangian. The integral of the spatial derivatives of  $u$  gives a constant, the Bogomol'nyi bound, and hence can be ignored. If one integrates the kinetic term over the entire plane, one sees it diverges logarithmically, so if  $\beta$  is a function of time, the solution has infinite energy.

Nonetheless, this is what we wish to investigate. We presume that the evolution takes place in a ball around the origin of size  $R$ . Up to a multiplicative constant, the effective or cutoff Lagrangian becomes

$$L = \int_0^R r dr \frac{r^2 (\partial_t f)^2}{(r^2 + f^2)^2} \quad (26)$$

which integrates to

$$L = \frac{(\partial_t f)^2}{2} \left[ \ln \left( 1 + \frac{R^2}{f^2} \right) - \frac{R^2}{f^2 + R^2} \right]. \quad (27)$$

For geodesics, energy is conserved, so

$$\frac{(\partial_t f)^2}{2} \left[ \ln \left( 1 + \frac{R^2}{f^2} \right) - \frac{R^2}{f^2 + R^2} \right] = \frac{c^2}{2}, \quad (28)$$

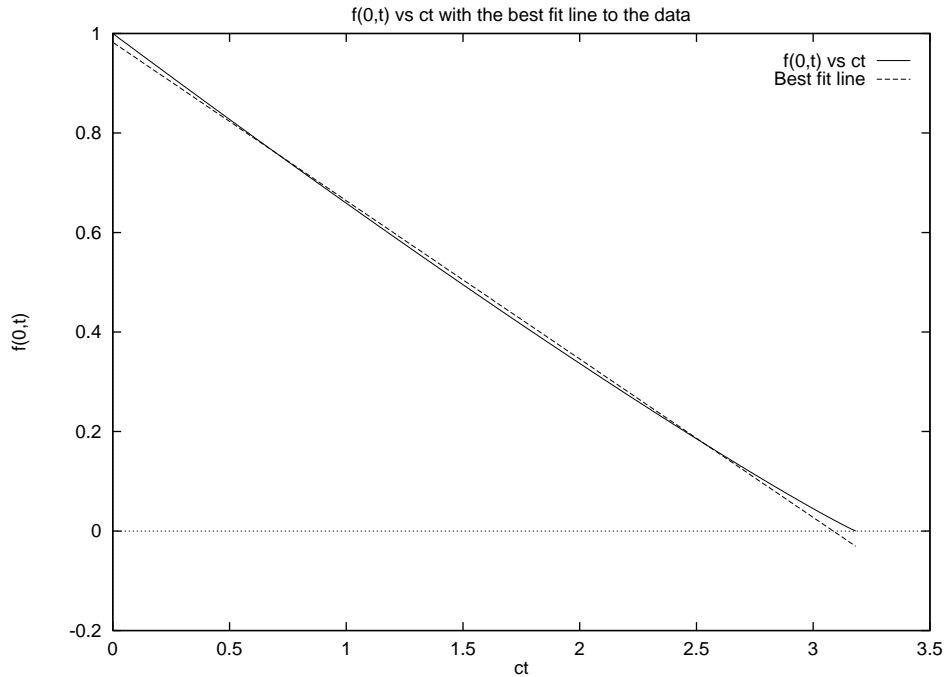


Figure 2: Predicted plot of  $f(0,t)$  vs  $ct$  for the cutoff Lagrangian with  $R = 100$  in the charge-one  $\sigma$ -model.

with  $c$  (and hence  $c^2/2$ ) a constant. Solving for  $\partial_t f$  we obtain

$$\partial_t f = \frac{c}{\sqrt{\left[ \ln \left( 1 + \frac{R^2}{f^2} \right) - \frac{R^2}{f^2 + R^2} \right]}}. \quad (29)$$

Since we are starting at some value  $f_0$  and evolving toward the singularity at  $f = 0$  this gives:

$$\int_{f_0}^{f(0,t)} df \sqrt{\ln \left( 1 + \frac{R^2}{f^2} \right) - \frac{R^2}{f^2 + R^2}} = \int_0^t c dt. \quad (30)$$

In the  $R \rightarrow \infty$  limit, as taken in [8], this gives linear evolution, *i.e.*, fast blowup. But this would violate the Shatah-Struwe theorem [10]. However, taking a finite value of  $R$  gives  $\sqrt{|\ln(t)|}$  corrections and slow blowup, in accordance with the theorem.

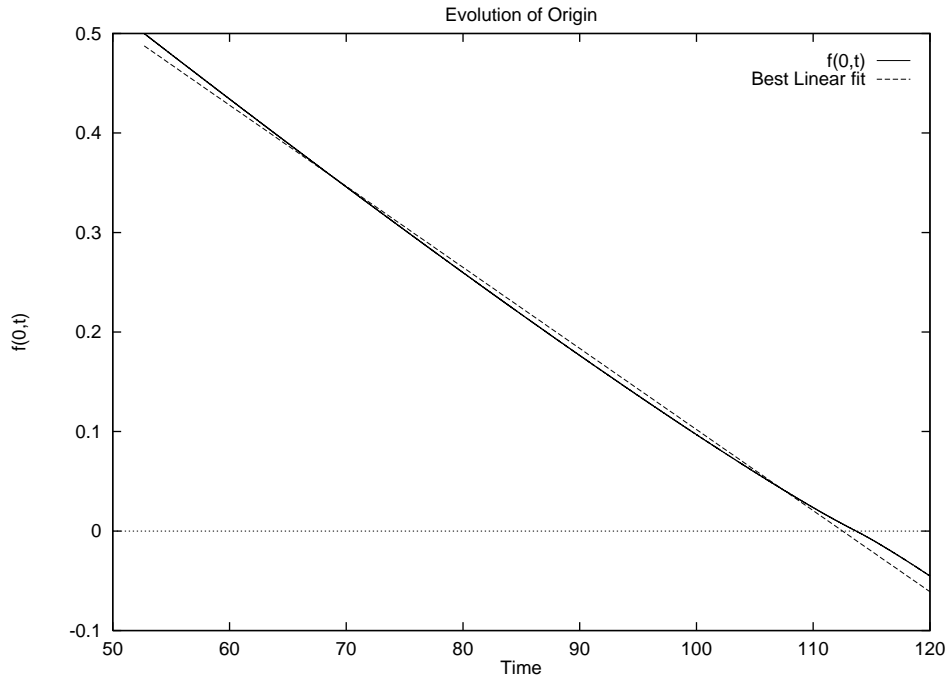


Figure 3: Plot of  $f(0,t)$  vs  $t$  for an actual trajectory in the charge-one  $\sigma$ -model. The slight nonlinearity is reminiscent of the prediction shown in Figure 2.

In equation (30), the integral on the right gives  $ct$ . The integral on the left can be evaluated numerically for given values of  $R$ ,  $f_0$  and  $f(0,t)$ . A plot can then be generated for  $ct$  vs.  $f(0,t)$ . What we really are concerned with is  $f(0,t)$  vs.  $t$ , but once the value of  $c$  is determined this can be easily obtained. One such plot with  $f_0 = 1.0$ ,  $R = 100$  of  $f(0,t)$  vs  $ct$  is given in Figure 2. This curve is not quite linear, as seen by comparison with the best fit line; both are plotted in Figure 2.

The scale invariance of this problem allows us to consistently take  $f_0 = 1.0$  without loss of generality, and the key dimensionless parameter is  $\partial_t f(0,0)$ . We compare this with the numerical computer model, which was run with various small velocities. The initial velocity is  $\partial_t f(r,0) = v_0$ . Another important input parameter is  $R_{max}$ , the largest value of  $r$  modeled, which is chosen large enough so that information from the origin cannot propagate out to the boundary and bounce back to the origin within the time to blowup. Other

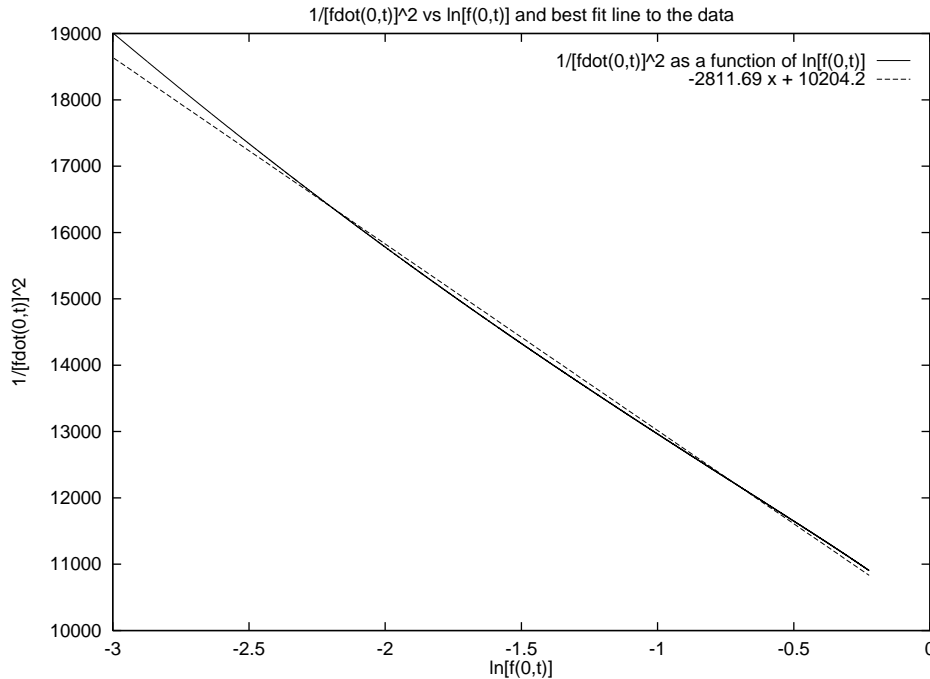


Figure 4: Actual plot of  $1/(\partial_t f(0,t))^2$  vs  $\ln(f(0,t))$  for the charge-one  $\sigma$ -model and the best fit line to this data. The cutoff Lagrangian predicts linear dependence, while the  $R \rightarrow \infty$  limit predicts that  $1/\partial_t f^2$  should be constant.

input parameters are  $\Delta r$  and  $\Delta t$ .

We track  $f(0,t)$  as it heads toward this singularity, and find that its trajectory is not quite linear, as seen in Figure 3. This is suggestive of the result obtained in the predictions for this model.

We want to check the legitimacy of the prediction (30), pictured in Figure 2. This requires a determination of the cutoff<sup>3</sup>  $R$  and the kinetic energy  $c^2/2$ . We already have  $f_0$  and  $f(0,t)$ . To determine  $R$  and  $c$ , observe from equation

<sup>3</sup>The Lagrangian cutoff  $R$  is not to be confused with  $R_{max}$ , the maximum value of  $r$  modeled numerically.  $R$  is a parameter of the geodesic approximation, not of the numerical integration.



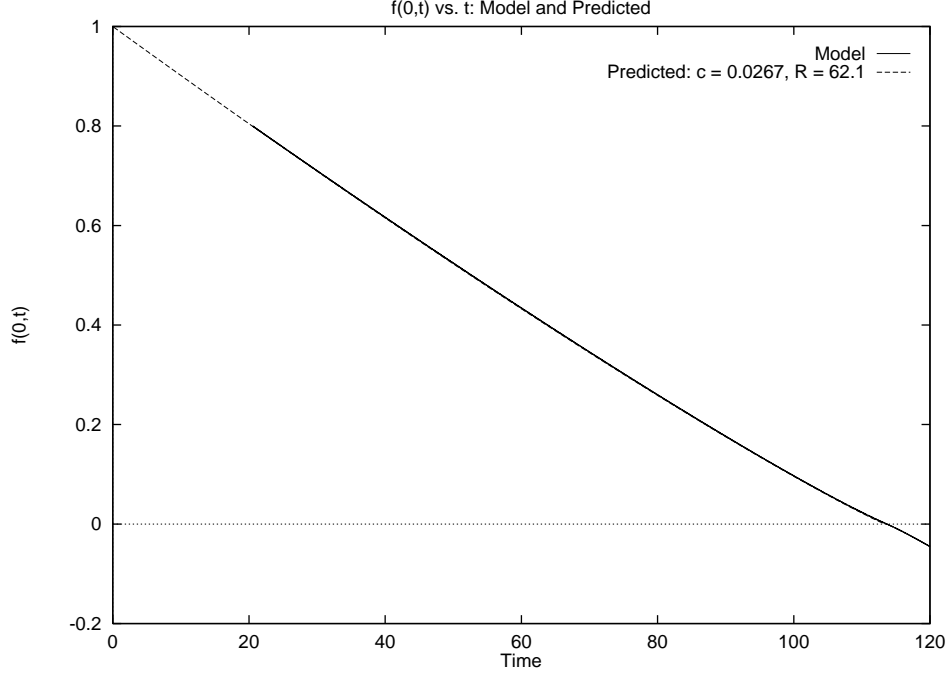


Figure 5: Comparison of the cutoff geodesic approximation to actual data in the charge-one  $\sigma$ -model. The predicted course of  $f(0, t)$  vs.  $t$  from equation (30) is practically indistinguishable from the actual trajectory.

(29) that:

$$\frac{1}{(\partial_t f)^2} = \frac{\left[ \ln \left( 1 + \frac{R^2}{f^2} \right) - \frac{R^2}{f^2 + R^2} \right]}{c^2} \quad (31)$$

Since  $R$  is large and  $f$  is small, we can rewrite equation (31) as

$$\frac{1}{(\partial_t f)^2} \approx \frac{[\ln(R^2) - \ln(f^2) - 1]}{c^2}. \quad (32)$$

The plot of  $\ln(f) = \ln(f(0, t))$  vs  $1/(\partial_t f)^2 = 1/(\partial_t f(0, t))^2$  should be linear with the slope  $= 2/c^2$  and the intercept  $= (2 \ln(R) - 1)/c^2$ . Such a plot is easily obtained from the data, and the parameters  $c$  and  $R$  are readily calculated.

Figure 4 is a plot of  $\ln(f(0, t))$  vs.  $1/(\partial_t f(0, t))^2$ , with initial conditions  $\Delta r = 0.01$ ,  $\Delta t = 0.001$ ,  $f_0 = 1.0$  and  $v_0 = -0.01$ . If the correct dynamics

Table 1: Best-fit parameters  $c$  and  $R$  as a function of  $v_0$ , with  $f_0 = 1.0$  for the charge-one  $\sigma$ -model.

$v_0$	$c$	$R$	
-0.005	0.0145	115	
-0.00667	0.0187	89	
-0.01	0.0263	53	
-0.0133	0.0342	49	(33)
-0.02	0.0485	34	
-0.03	0.0683	25	
-0.05	0.104	17	
-0.06	0.121	15	

were given by the  $R \rightarrow \infty$  limit of equation (30), this graph would be of a horizontal line, since the velocity would be unchanging. On the other hand, if equation (30) is correct with  $R$  finite, we should get a line with nonzero slope. It is easily seen that the plot of  $\ln(f(0, t))$  vs.  $1/(\partial_t f(0, t))^2$  is nearly a linear relationship, as predicted by the cutoff Lagrangian, but is not quite a straight line. This may indicate that the effective values of  $R$  and  $c$  are themselves changing slowly with time.

The best fit line to this data has slope -2810 and intercept 10200, corresponding to  $c = 0.0267$  and  $R = 62.1$ . Using these values of  $c$  and  $R$  in the calculation of equation (30), we obtain the plot of  $f(0, t)$  vs  $t$  given in Figure 5. This is overlaid with the model data for  $f(0, t)$  vs.  $t$  for comparison. These two are virtually indistinguishable.

We have seen that modifying the geodesic approximation by applying a fixed and finite cutoff greatly improves its accuracy. Moreover, corrections to linear behavior are seen to be logarithmic, not power-law. However, we have not yet demonstrated any predictive power, since the cutoff was deduced from the data only after the fact. What is needed is an understanding of how the dynamically generated cutoff  $R$  (and the kinetic energy  $c^2/2$ ) vary with initial conditions.

Table 1 gives the best-fit values for  $c$  and  $R$  as a function of the initial velocity  $v_0$ , under the initial conditions  $f_0 = 1.0$ ,  $\Delta r = 0.01$  and  $\Delta t = 0.001$ .

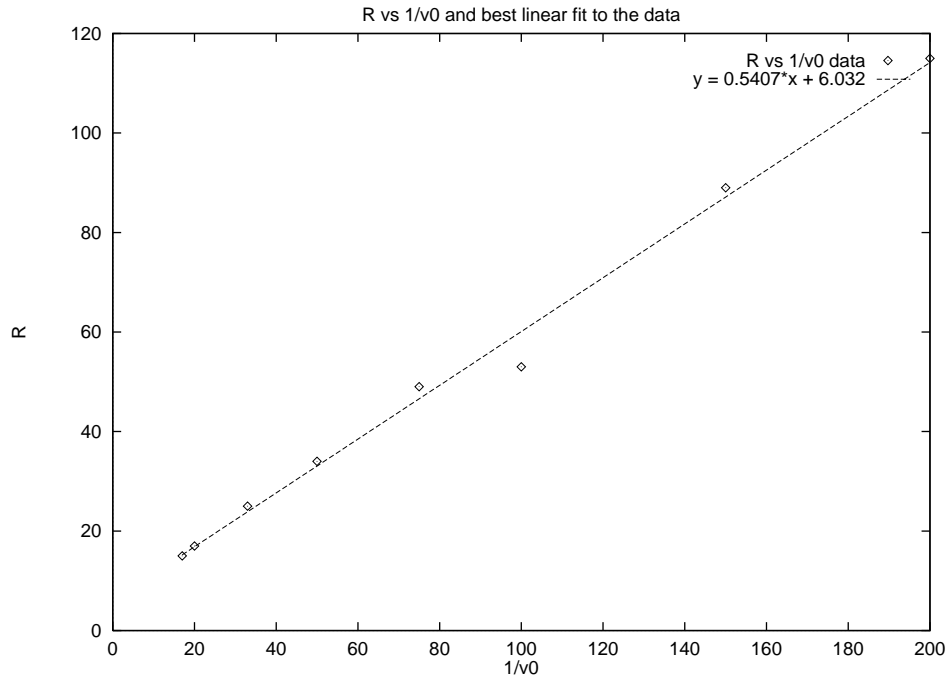


Figure 6: The dynamical cutoff  $R$  grows linearly with  $1/v_0$  in the charge-one  $\sigma$ -model.

$R$  is roughly linear in  $1/v_0$ , with best-fit line

$$R = \frac{0.5407}{v_0} + 6.032. \quad (34)$$

This fit is shown in Figure 6. A linear fit with  $1/v_0$  makes sense, since the time to blowup is itself of order  $1/v_0$ .  $R$  is roughly half the radius of the light cone at  $t = 0$ .

Next we consider the shape of the lump as we approach blowup. That is, what is  $f(r, T)$  with  $T$  fixed? The geodesic approximation indicates that  $f(r, t)$  should be independent of  $r$ , but this is only approximately true. The graph of  $f(r, t)$  versus  $r$  stays close to horizontal, although there is some slope downward as time increases. This is shown in Figure 7.

Making a closer inspection of the time profiles  $f(r, T)$ , as in Figure 7, we observe that the initial part of the data is close to a hyperbola as seen in Figure 8. This fit is close, but not nearly as close as those for profiles in the

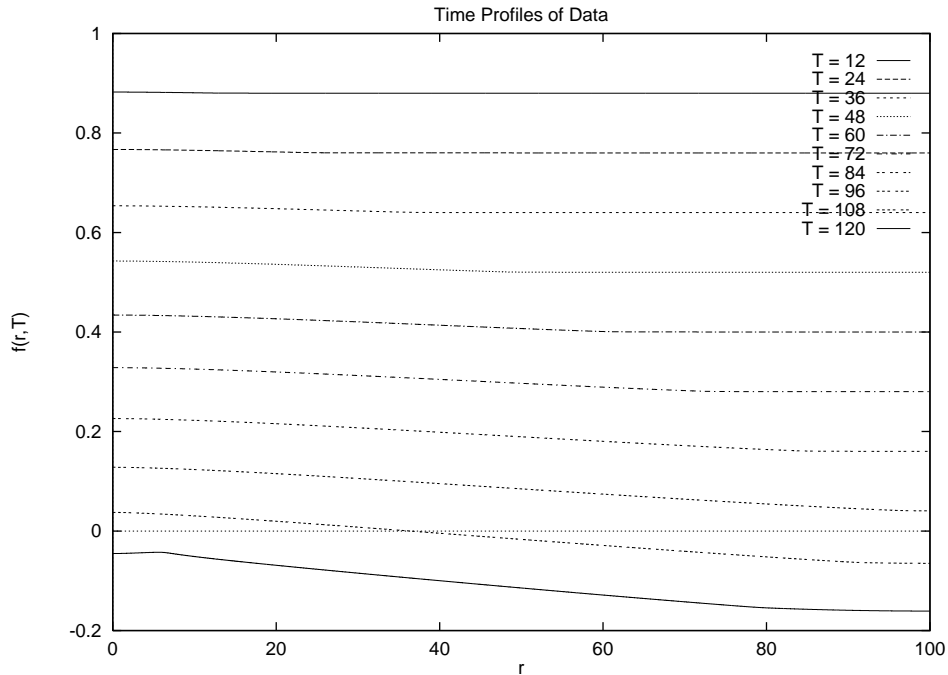


Figure 7: Time slices  $f(r, T)$  for the charge-one  $\sigma$ -model.

charge-two sector of the  $S^2$   $\sigma$ -model or the (4+1)-dimensional Yang-Mills Model, below. While the asymptotic conditions for the hyperbola are not consistent with those of a solution to this equation, this form need only be assumed on a ball about the origin, outside of which the function is of the form  $f(r > R, T) = \alpha$ .

## 4.2 The Charge-Two $S^2$ $\sigma$ -Model

Equation (1) gives us the Lagrangian for the general version of this problem. We are using

$$u = \frac{\lambda(t)}{z^2} \quad (35)$$

for our evolution, and via the geodesic approximation we restrict the Lagrangian integral to this space, to give an effective Lagrangian, as we did in the previous section. The integral of the spatial derivatives of  $u$  gives a constant, and hence can be ignored. Unlike the charge-one  $\sigma$ -model, this

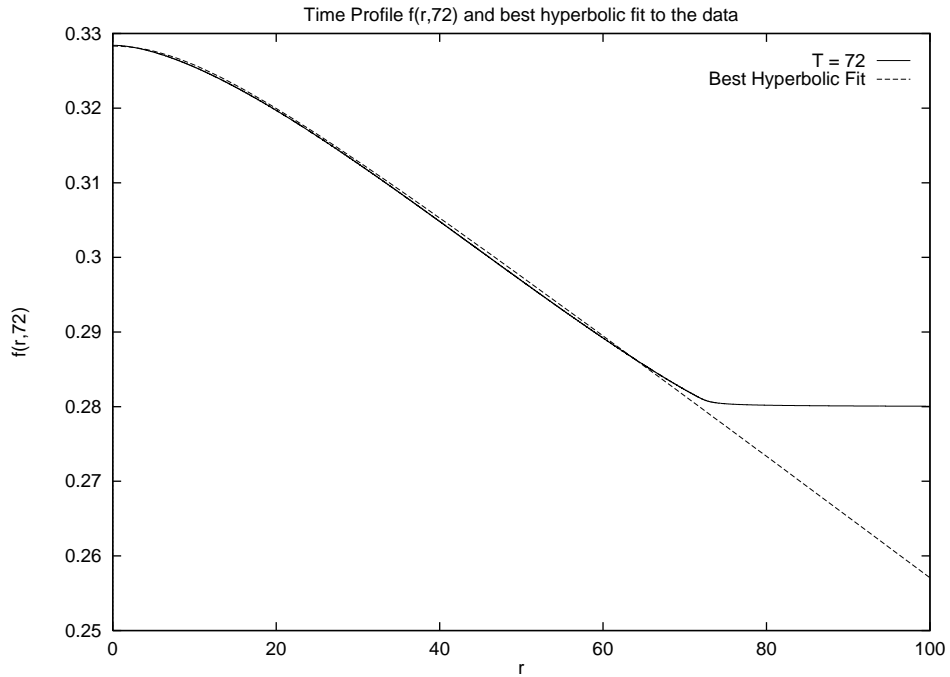


Figure 8: Time slices for the charge-one  $\sigma$ -model evolve a hyperbolic bump at the origin. The transition from a hyperbola to a horizontal line occurs at  $r = T$ .

Lagrangian does not have an infrared divergence, and there is no need to apply a cutoff. Up to a multiplicative constant, the effective Lagrangian is

$$L = \int_0^\infty r dr \frac{r^4 (\partial_t \lambda)^2}{(r^4 + \lambda^2)^2} = \frac{(\partial_t \lambda)^2 \pi}{8\lambda}. \quad (36)$$

By conservation of energy,

$$\partial_t \lambda = 2c_1 \sqrt{\lambda}, \quad (37)$$

for some constant  $c_1$ , and we integrate to obtain

$$\lambda(t) = (c_1 t + c_2)^2, \quad (38)$$

which we rewrite as

$$\lambda(t) = p(t - t_0)^2. \quad (39)$$

Table 2: Parameters for best fit parabola to  $f(0, t)$  vs. initial data  $f_0$  and  $v_0$  for the charge-two  $S^2$   $\sigma$ -model.

$f_0$	$v_0$	$t_0$	$p$	
1.0	-0.01	200	0.0000250	
1.0	-0.02	100	0.0000998	
1.0	-0.03	67	0.000224	
1.0	-0.04	50	0.000398	(40)
1.0	$\frac{-\sqrt{2}}{100}$	$100\sqrt{2}$	0.0000499	
1.0	$\frac{-0.01}{\sqrt{2}}$	$200\sqrt{2}$	0.0000125	
1.0	$\frac{-0.01}{\sqrt{3}}$	$200\sqrt{3}$	0.00000833	

Equation (39) is how we predict that  $f(0, t)$  will evolve.

As before, the scale invariance of the model allows us to fix  $f_0$ , and the other input parameters are the same as before. A typical evolution of  $f(0, t)$  looks like that given in Figure 9. (That figure is actually a trajectory for the Yang-Mills model, but the results from these two models are essentially the same.) In every case, the trajectory of  $f(0, t)$  fits a parabola of the form  $p(t - t_0)^2$  almost perfectly. The dependence of the parabolic parameters  $p$  and  $t_0$  on initial velocity  $v_0$  is given in Table 2. In all cases we took  $f(r, 0) = f_0 = 1.0$ ,  $\partial_t f(r, 0) = v_0$ ,  $\Delta r = 0.025$  and  $\Delta t = 0.001$ , and in all cases we obtain

$$t_0 = \frac{2}{|v_0|} \quad \text{and} \quad p = \frac{v_0^2}{4}. \quad (41)$$

The predictability of the parameters from Table 2, and the closeness of the parabolic fits indicate there is no correction needed to the predictions of the geodesic approximation.

With the evolution of  $f(0, t)$  taken care of, we consider the shape of the time slices  $f(r, T)$  for a given fixed  $T$ . The geodesic approximation suggests that the graph of  $f(r, T)$ , which starts horizontal, should remain horizontal. Instead, an elliptical bump forms at the origin, as seen in Figure 10. (That figure is also from the Yang-Mills model, which exhibits essentially identical behavior).

If we describe the elliptical bump by the equation

$$\frac{x^2}{a^2} + \frac{(y - k)^2}{b^2} = 1, \quad (42)$$

then the parameters  $a$ ,  $b$  and  $k$  evolve as

$$a = t \quad (43)$$

$$b = \frac{v_0^2}{4} t^2 \quad (44)$$

$$k = 1.0 + v_0 t. \quad (45)$$

The growth of this ellipse suggests that the curve is trying to adjust from a horizontal line to a parabola

$$f(r, t) = \rho r^2 + h, \quad (46)$$

where

$$\rho = -\frac{1}{2} \frac{d^2 y}{dx^2} = -\frac{b}{2a^2} = -\frac{v_0^2}{8}. \quad (47)$$

To test this, we began runs with initial data

$$f(r, 0) = 1 - v_0^2 r^2 / 8; \quad \partial_t f(r, 0) = -v_0. \quad (48)$$

for various values of  $v_0$ . The time slices of these runs retained a parabolic profile, as shown (for the Yang-Mills model) in Figure 11. That is, we expect

$$f(r, t) \simeq -\frac{v_0^2}{8} r^2 + \frac{v_0^2}{4} \left( t - \frac{2}{|v_0|} \right)^2. \quad (49)$$

Substituting this closed-form expression into (9), we find the error is

$$\frac{v_0^6}{64} r^4 - \frac{v_0^6}{32} r^2 \left( t - \frac{2}{|v_0|} \right)^2. \quad (50)$$

Within a fixed radius, and for small  $v_0$ , this error remains small for all time. However, the parabolic fit cannot be extended out arbitrarily far, especially insofar as the profile (46) has logarithmically divergent potential energy.

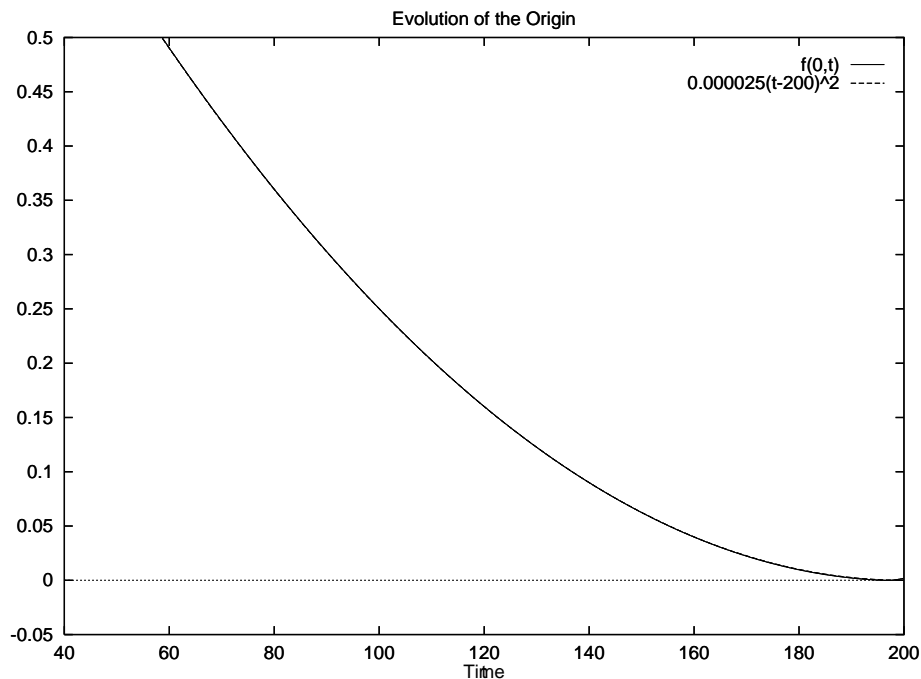


Figure 9: Sample trajectory of  $f(0, t)$  vs.  $t$  in the Yang-Mills model. The actual trajectory is almost exactly parabolic.

### 4.3 The (4+1)-Dimensional Yang-Mills Model

Equation (11) gives us the Lagrangian for the general version of this problem. We are using

$$A = \frac{1}{2} \left\{ \frac{\bar{x}dx - d\bar{x}x}{f + r^2} \right\} \quad r = \sqrt{x_1^2 + x_2^2 + x_3^2 + x_4^2}, \quad (51)$$

and we apply the geodesic approximation. Restricting the Lagrangian to the moduli space gives us an effective Lagrangian. The portion of the integral given by

$$- \frac{1}{4} \int_{\mathbb{R}^4} |F_{ij}|^2 d^4\vec{x} \quad (52)$$

represents the potential energy and integrates to a topological constant, hence it may be ignored, as in the study of the  $S^2$   $\sigma$ -model. We need to calculate

$$L = \frac{1}{2} \int_{\mathbb{R}^4} |\partial_t A_i|^2 d^4\vec{x}. = \int_{\mathbb{R}^4} \frac{3r^2(\partial_t f)^2}{(f + r^2)^4} d^4\vec{x} = \text{const.} \times \frac{(\partial_t f)^2}{f}. \quad (53)$$



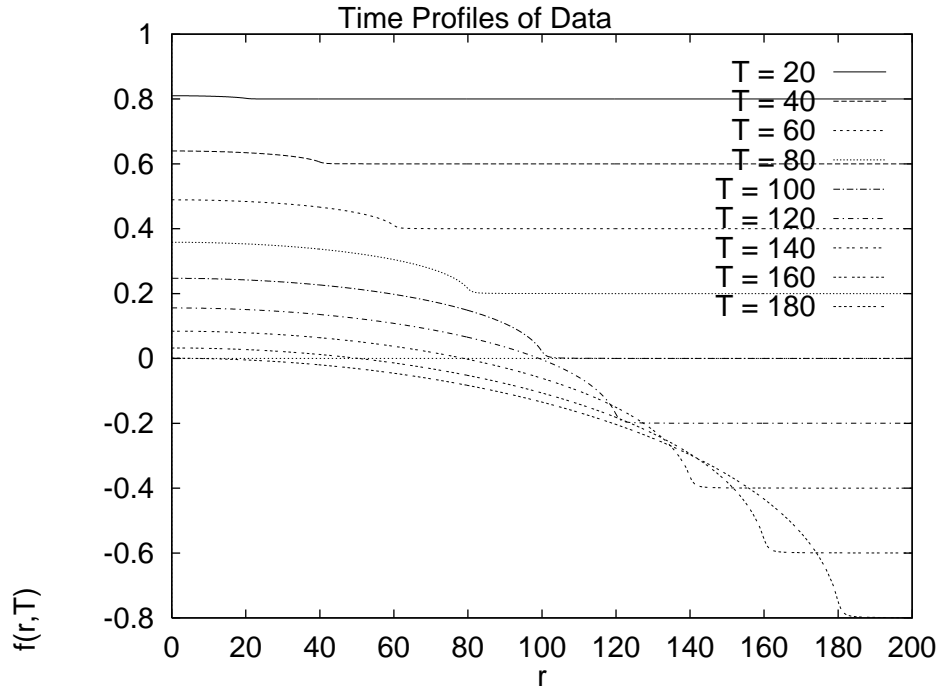


Figure 10: Time slices  $f(r, T)$  for the Yang-Mills model evolve an elliptical bump at the origin. The edge of the bump is always at  $r = T$ .

Since energy is conserved,  $\partial_t f$  is proportional to  $f^{1/2}$ , and we integrate to get

$$f = p(t - t_0)^2. \quad (54)$$

In short, the predicted evolution is identical to that of the charge two  $\sigma$ -model.

A typical evolution of  $f(0, t)$  is given in Figure 9. In this figure, the graph of  $0.000025(t - 200)^2$  neatly overlays the graph of  $f(0, t)$ . This picture represents the evolution where  $f_0 = 1.0$  and  $v_0 = -0.01$ .

If we now look at the evolution of the initial line,  $f(r, 0) = f_0$ , we obtain the same striking result as with the charge-two  $S^2$   $\sigma$ -model. The initial line,  $f(r, 0) = f_0$ , evolves an elliptical bump at the origin that grows as time passes. Figure 10 shows this behavior. The clear indication here is that corrections to the profile are quadratic. The elliptical bumps can be modeled exactly as before. Also as before, this suggests that we look for an approximate solution of the form  $f(r, t) = \rho(t)r^2 + h(t)$ . Calculating from the general

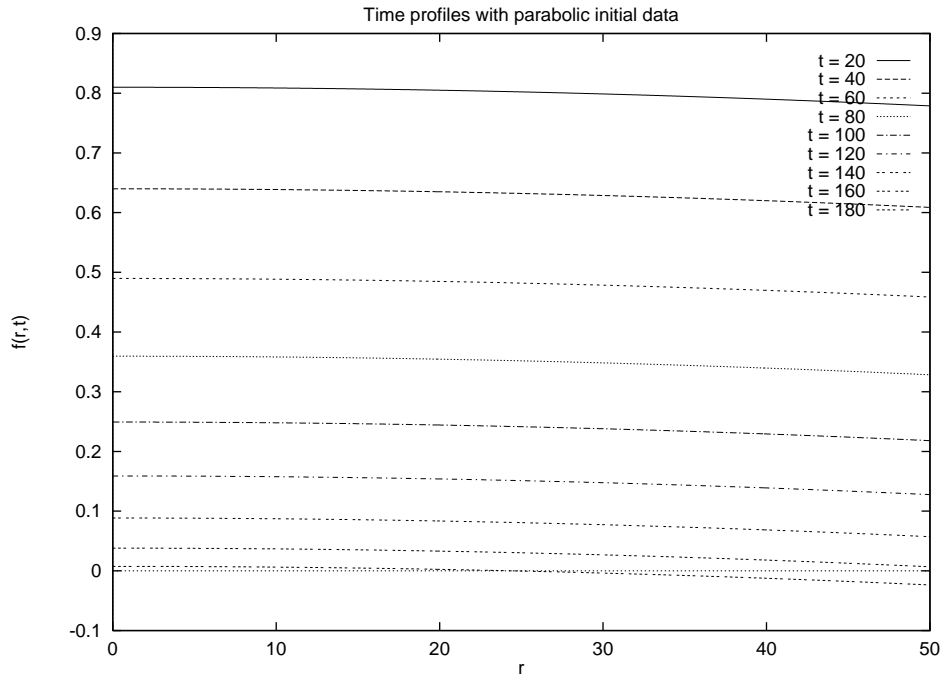


Figure 11: With parabolic initial conditions, the time slices in the (4+1)-dimensional Yang-Mills model do not form bumps, but instead remain parabolic.

form of our ellipse in (42) we get the same results for  $\rho$  as in (47), and  $h$  should evolve the same way as  $f(0, t)$ . When a run is started with this initial data  $\partial_t f_0 = v_0 = -0.01$ ,  $f(r, 0) = 1.0 - \rho r^2$  and  $\rho = -\frac{v_0^2}{8} = -0.0000125$ , the time slices of the data retain a parabolic profile. This is shown in Figure 11. The curvature of the parabola at the origin, as measured by the parameter  $\rho$  from equation (46) changes by less than 1 part in 100 during the course of this evolution.

The general form of a parabolic  $f(r, t)$  is the same as in equation (49). If we substitute this into the partial differential equation (17), we get an error of

$$2 \left( \frac{v_0^2}{4} \right)^2 r^2. \quad (55)$$

Since our concern is the adiabatic limit,  $v_0$  is always chosen to be small, and this difference goes to zero quickly in the adiabatic limit.

The form of the connection  $A$  given by this parabolic model is

$$A(r, t) = \frac{1}{2} \left\{ \frac{\bar{x}dx - d\bar{x}x}{\left(1 - \frac{v_0^2}{8}\right)r^2 + \frac{v_0^2}{4}\left(t - \frac{2}{|v_0|}\right)^2} \right\}. \quad (56)$$

This is close to the connection  $A$  given by the geodesic approximation multiplied by an overall factor. This form suggests a relativistic correction.

## 5 Conclusions

We have studied the time evolution of solutions towards a singularity in the charge-one  $S^2$   $\sigma$ -model, the charge-two  $S^2$   $\sigma$ -model and the (4+1)-dimensional Yang-Mills model. We use a simple and robust numerical scheme to do so, for which the stability has been verified. The importance of the stability analysis is that we have no problem trying to separate real effects from numerical artifacts.

In the charge-one  $\sigma$ -model, the geodesic approximation is ill-defined due to the divergence of the Lagrangian. A theorem of [10] tells us that there is no fast blowup in this model. The divergence of the geodesic approximation is solved by cutting off the Lagrangian at a radius  $R < \infty$ . In the  $R \rightarrow \infty$  limit of this cut-off Lagrangian, we have a prediction for linear evolution, which would be fast blowup in violation of the theorem in [10]. However, the cut-off Lagrangian itself is extremely accurate in predicting the shrinking of lumps toward the singularity in this model. This evolution is close to linear with complicated logarithmic corrections (equation (30)) going approximately as  $\sqrt{\ln(t_0 - t)}$ . Corrections from linear are not power-law, nor power-law corrected by a logarithm, as suggested in [8].

We model the charge-two  $\sigma$ -model and the (4+1)-dimensional Yang-Mills model to provide a comparison to our charge-one  $S^2$   $\sigma$ -model results. We verify the belief that the charge two  $S^2$   $\sigma$ -model is similar to the (4+1)-dimensional Yang-Mills model; the numerical results show that the two models are almost identical in behavior. There is no theorem restricting fast blowup in either of these models, and we find fast blowup as predicted by the geodesic approximation in both. The numerical models' evolution toward the singularity is in lock step with prediction, and no corrections are needed to this order. Since the stability analysis of the numerical schemes in the

charge-one  $S^2$   $\sigma$ -model and the Yang-Mills model is similar, the accuracy of the numerics to prediction in the charge-two  $S^2$   $\sigma$ -model and Yang-Mills model provide a accuracy scale on which to judge the charge-one  $S^2$   $\sigma$ -model.

In addition to modeling the evolution toward the singularity, we also can characterize the shape of the profiles of the lumps with the time variable fixed. In the geodesic approximation, with the rotationally symmetric functions we have chosen to model, the predicted evolution in all three cases was  $f(r, t) = \alpha(t)$ . The actual profiles in all three cases have quadratic corrections.

### **Acknowledgments**

We thank Martin Speight for some extremely helpful suggestions. This work was partially supported by the Texas Advanced Research Program.

## References

- [1] M. F. Atiyah. *Geometry of Yang-Mills Fields*. Accademia Nazionale Dei Lincei Scuola Normale Superiore, 1979.
- [2] Piotr Bizoń, Tadeusz Chmaj and Zbislav Tabor. Formation of singularities for equivariant 2+1 dimensional wave maps into two-sphere. *Preprint, xxx.lanl.gov*, math-ph/0011005, 2000.
- [3] Theodora Ioannidou. Soliton dynamics in a novel discrete  $O(3)$   $\sigma$ -model in (2+1) dimensions. *Nonlinearity*, 10:1357–1367, 1997.
- [4] Robert Leese. Low-energy scattering of solitons in the  $\mathbb{CP}^1$  model. *Nuclear Physics B*, 344:33–72, 1990.
- [5] Robert A. Leese, Michel Peyrard, Wojciech J. Zakrzewski. Soliton stability in the  $O(3)$   $\sigma$ -model in (2+1) dimensions. *Nonlinearity*, 3:387–412, 1990.
- [6] Jean Marie Linhart. Numerical investigations of singularity formation in non-linear wave equations in the adiabatic limit. Dissertation, Mathematics Department, The University of Texas at Austin, Austin, TX 78712 USA, May 1999. *Available at xxx.lanl.gov*.
- [7] N.S. Manton. A remark on the scattering of BPS monopoles. *Phys. Lett.* **110B**: 54–56, 1982.
- [8] B. Piette and W. J. Zakrzewski. Shrinking of solitons in the (2+1)-dimensional  $S^2$  sigma model. *Nonlinearity*, 9:897–910, 1996.
- [9] W. H. Press, S. A. Teukolsky, W. T. Vetterling and B. P. Flannery. *Numerical Recipes in C*. Cambridge University Press, 1992.
- [10] J. Shatah and M. Struwe. *Geometric Wave Equations*. Courant Lecture Notes 2. New York University, 1998.
- [11] J. M. Speight. Low-energy dynamics of a  $\mathbb{CP}^1$  lump on the sphere. *J. Math. Phys.*, 36:796, 1995.
- [12] J. M. Speight. Lump dynamics in the  $\mathbb{CP}^1$  model on the torus *Commun. Math. Phys.* 194:513, 1998.

- [13] D. Stuart. The geodesic approximation for the Yang–Mills–Higgs equations. *Commun. Math. Phys.*, 166:149–190, 1994.
- [14] R. S. Ward. Slowly-moving lumps in the  $\mathbb{C}\mathbb{P}^1$  model in (2+1) dimensions. *Physics Letters*, 158B(5):424–428, 1985.
- [15] Wojciech J. Zakrzewski. Soliton-like scattering in the  $O(3)$   $\sigma$ -model in (2+1) dimensions. *Nonlinearity*, 4:429–475, 1991.